Journal of Systems Engineering and Electronics
Vol. PP, No. 99, September 2023, pp.1 – 11

Fast measurement and prediction method for electromagnetic susceptibility of receiver

CHEN Yan [1,2], LU Zhonghao [1,*], and LIU Yunxia [2]

1. State Key Laboratory of Complex Electromagnetic Environment Effects on Electronics and Information System, College of Electronic Science and Technology, National University of Defense Technology, Changsha 410073, China;
2. State Key Laboratory of Astronautic Dynamics, Xi'an 710043, China

Abstract: Aiming at evaluating and predicting rapidly and accurately a high sensitivity receiver's adaptability in complex electromagnetic environments, a novel testing and prediction method based on dual-channel multi-frequency is proposed to improve the traditional two-tone test. Firstly, two signal generators are used to generate signals at the radio frequency (RF) by frequency scanning, and then a rapid measurement at the intermediate frequency (IF) output port is carried out to obtain a huge amount of sample data for the subsequent analysis. Secondly, the IF output response data are modeled and analyzed to construct the linear and nonlinear response constraint equations in the frequency domain and prediction models in the power domain, which provide the theoretical criteria for interpreting and predicting electromagnetic susceptibility (EMS) of the receiver. An experiment performed on a radar receiver confirms the reliability of the method proposed in this paper. It shows that the interference of each harmonic frequency and each order to the receiver can be identified and predicted with the sensitivity model. Based on this, fast and comprehensive evaluation and prediction of the receiver's EMS in complex environment can be efficiently realized.

Keywords: electromagnetic susceptibility (EMS), receiver, dual-channel multi-frequency, nonlinear response, frequency domain, power domain.

DOI: 10.23919/JSEE.2023.000127

1. Introduction

The radio receiver is one of the most important devices of a wireless transceiver system. In the complex electromagnetic environment, especially large platforms or systems such as aircraft, satellites, and high-speed railways, or ships with dense high-power radiation sources and numerous high-sensitivity receivers, multiple signals with high power are usually coupled to the input port of the receivers [1−3]. These signals may cause linear and nonlinear effects and interference in the receiver on receiving paths [4,5]. Furthermore, these interferences can lead to a series of electromagnetic compatibility (EMC) problems, such as narrowed effective reception bandwidth, distorted signal waveform and image, time drifting, and increased noise [6,7], leading to system performance degradation or even malfunction. To solve EMC problems and improve the stability and reliability of large platforms or systems, it is necessary to strictly control the use of frequency equipment and improve receiver sensitivity [8−11]. All of these require a comprehensive understanding of the adaptability of receivers to electromagnetic environment [12−14].

Identifying all existing interference paths promptly and predicting the potential influence accurately of the receiver is a tough task [15,16]. The existing tools and methods cannot effectively solve it. Using the traditional two-tone test, only the third-order intermodulation distortion [17−19] and other nonlinear immunity models with limited frequency points in- or out-band of the receiver [20−24] can be obtained. Due to the complex electromagnetic environment surrounding the electronic equipment on large platforms or in complex systems, signal components with various frequencies and powers are likely to be input to the receiver and cause more interference effects [25]. Therefore, a sensitivity test should be carried out in such an environment, simulating a sufficient number of possible signals as test excitation signals [26]. Thus, it is far from enough to obtain nonlinear characteristics with a two-tone test for finite frequency points. Moreover, classical characteristics (frequency selectivity, third-order intermodulation point, 1 dB compression point, spurious free dynamic range, etc.) used to describe the nonlinearity are insufficient for EMC analysis and prediction. Therefore, comprehensive identification of receiver parameters and scientific characterization of its sensiti-

Manuscript received July 30, 2021.
*Corresponding author.
This work was supported by the National Natural Science Foundation of China (62071473).

vity is necessary for effective assessment of the EMC condition and prediction of the receiver system.

Aiming at the comprehensive, rapid, and accurate interpretation and prediction of receiver electromagnetic susceptibility (EMS), this paper proposes a method for measuring and predicting receiver interference characteristics and interference sensitivity using different frequency combinations based on dual-channel multi-frequency test method. In the following sections, the implementation process, data processing, and prediction model of the proposed method are described in detail. In addition, the feasibility and reliability of the proposed method are verified by an experiment on a radar receiver.

2. System fundamental

In this section, the framework of the measurement and analysis method is illustrated in detail. As shown in Fig. 1, the measurement and forecast system contains two subsystems, one for measuring the response of the receiver, and the other for data post-processing and prediction. RF_{in} represents the input radio frequency (RF) and IF_{out} represents the output intermediate frequency (IF).

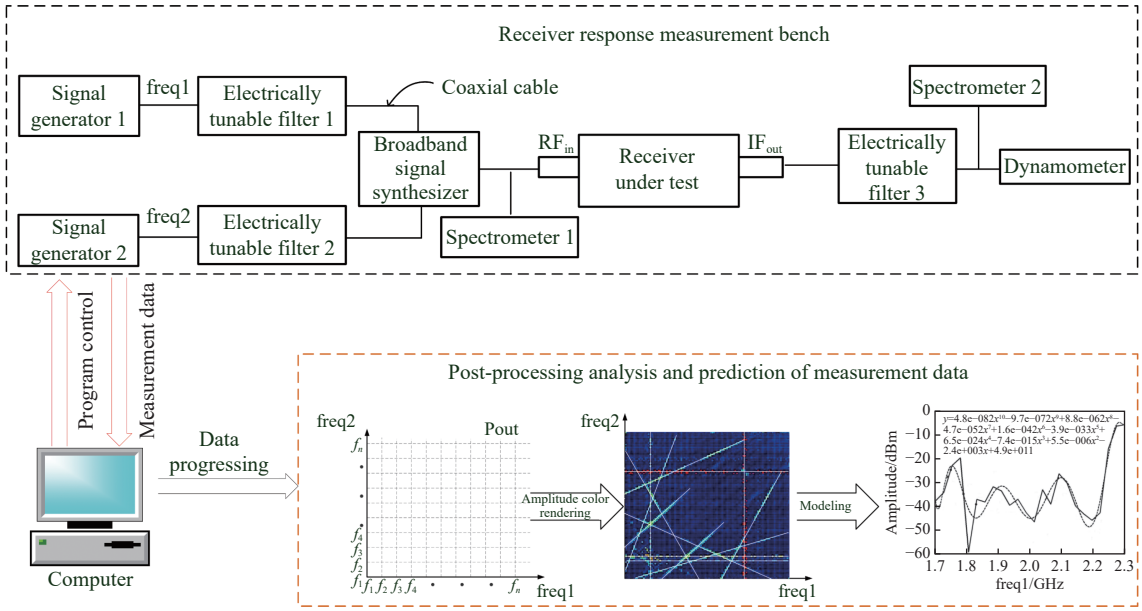

Fig. 1 Framework of measurement and prediction of the receiver EMS driven by two RF signals

2.1 Receiver response measurement bench

The subsystem of receiver response measurement bench is mainly used to test the input and output signal of the receiver. It comprises the signal generator, electrically tunable filter, signal synthesizer, spectrometer, and dynamometer. The equipment is connected by coaxial and driven by control program on the computer. The functions of each instrument or module in the measuring system are listed below.

(i) The two signal generators are used to generate two original excitation signals.

(ii) The electrically tunable filters 1 and 2 work as the narrow-band and band pass filter, under program control, which can adjust the center frequency to the frequency generated by a corresponding signal generator. Thus, the frequency purity of the signal source is well ensured by filtering out the harmonic and clutter components.

(iii) Considering that the band of test frequency is generally wide, the broadband signal synthesizer is chosen, which is used to mix two original signals generated by signal generators into one combined signal to excite the receiver.

(iv) By coupling a small portion of the synthetic signal at the output port of the broadband signal synthesizer, spectrometer 1 is used to monitor the excitation signal parameters (e.g. frequency, power, harmonic) to guarantee that the signal characteristics satisfy test requirements.

(v) The electrically tunable filter 3 works as the band pass filter. Its passband bandwidth is consistent with IF bandwidth.

(vi) By coupling a small portion of the output signal from the electrically tunable filter 3, the spectrometer 2 is mainly used to monitor the frequency of IF output response signal. Its monitoring bandwidth should be set in consistent with the IF bandwidth of the receiver.

(vii) The dynamometer is used to measure the power of the IF output response. The output data is recorded and

stored in a computer.

Cooperating with the above devices, measurement with control will be carried out in the following processes.

(i) Set the two independent signal generators with the same frequency sweep range and sweep step and generate signals in frequency scanning.

(ii) Frequency combination scanning mode is shown in Fig. 2. When time changes from 0 to t_1, fix frequency of signal generator 1 (freq1) as f_1, and gradually change frequency of signal generator 2 (freq2) from f_1 to f_n. At the same time, record the power of IF output power P_{out} each time freq2 changes.

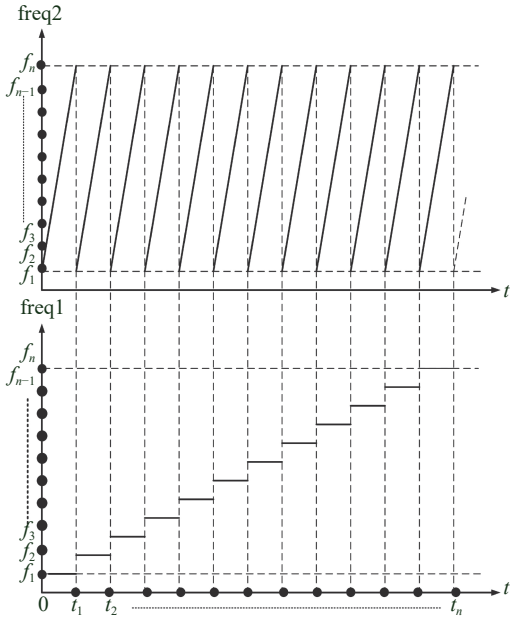

Fig. 2 Schematic of dual-channel and multi-frequency signal scanning

(iii) After signal generator 2 completes scanning at all frequency points, signal generator 1 jumps to the next frequency f_2 and keeps it. Then signal generator 2 operates frequency scanning again from f_1 to f_n. P_{out} at each frequency point is recorded at the same time.

(iv) Continue steps the second and third until signal generator 1 covers all frequency points set in the first step from f_1 to f_n.

2.2 Data post-processing analysis and prediction

This subsystem firstly interprets and discriminates the interference response imbed in the measurement and test result, i.e., the interpretation of the lines of similar colors in the color graph (as shown in Fig.1). Then the nonlinear response model is obtained by modeling the test data at finite frequency points, which can be used to predict the immunity of the receiver at continuous frequencies.

2.2.1 Interpretation and analysis of interference response

Using the real-time test data stored in random access memory (RAM), we can get the numerical matrix of P_{out} at each frequency combination point and plot the P_{out} numerical matrix. As shown in Fig. 1, by using the same frequency scale for horizontal and vertical coordinates, and calling "surf" function in Matlab function library to render the IF response amplitude using different colors, lines representing different interferences can be extracted.

As shown in Fig. 3, IF output response data is presented in the rectangular coordinate system with $\{f_1, f_2\}$ as the coordinate axes. The response frequency points corresponding to the same interference path will be connected in line. Different lines formed in Fig. 3 represent different interference paths [27].

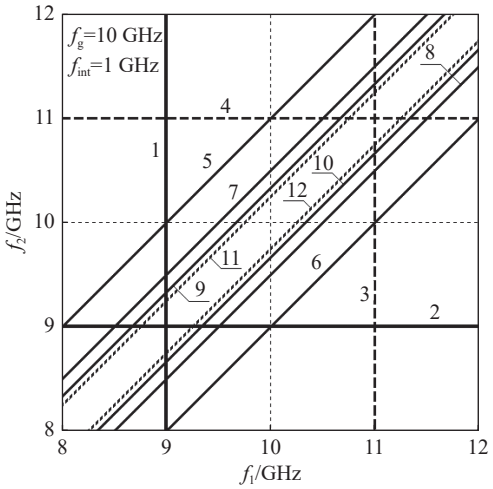

(a) Even-order intermodulation response of the typical single-frequency superheterodyne receiver

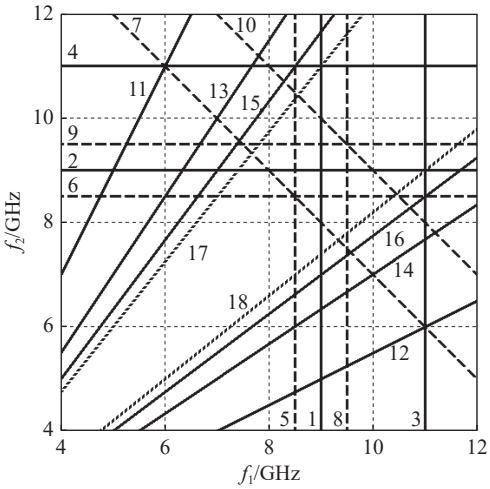

(b) Interference response of single-frequency superheterodyne receiver with adjustable RF amplifier

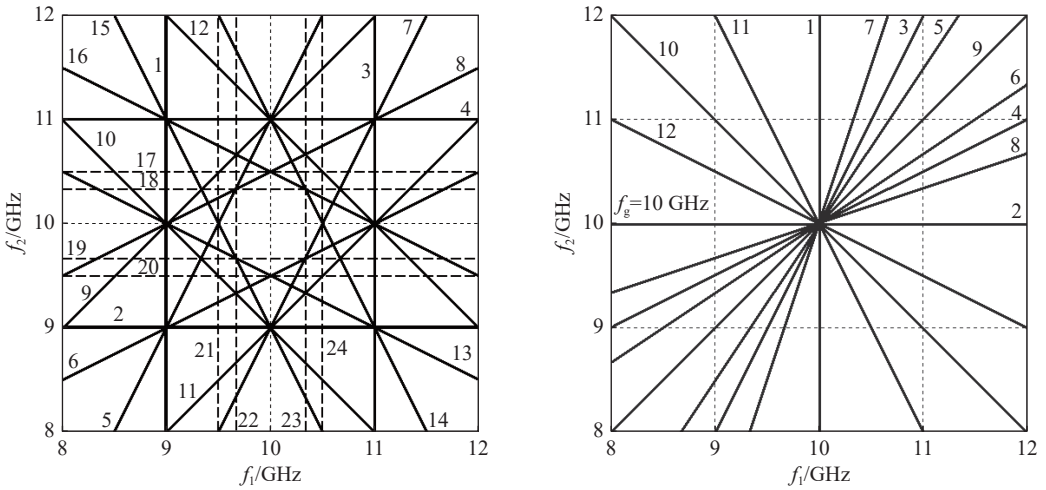

(c) Interference response of single-frequency superheterodyne receiver with mixer

(d) Interference response of direct conversion receiver

Fig. 3 IF interference response paths of a superheterodyne receiver

In order to interpret these lines, k_1 and k_2 are defined as the harmonic orders of the two original signals f_1 and f_2, k_g as the harmonic order of the local oscillator signal f_g, k_{int} as the type of frequency conversion (k_{int}=1 represents frequency up-conversion while k_{int}=−1 represents frequency down-conversion), and f_{int} as IF frequency [28].

For different types of superheterodyne receivers, the parameters satisfy the following constraints.

Constraint 1 Single-superheterodyne receiver:

$$\begin{cases} k_1 f_1 + k_2 f_2 = k_g f_g + k_{\text{int}} f_{\text{int}} \\ k_1, k_2 = 0, \pm 1, \pm 2, \cdots \\ k_g = 0, 1, 2, \cdots \\ k_{\text{int}} = \pm 1 \\ \min\{|k_1| + |k_2|\} = 1 \\ L = |k_1| + |k_2| \end{cases}.$$

Constraint 2 Secondary-superheterodyne receiver:

$$\begin{cases} k_1 f_1 + k_2 f_2 = k_{g1} f_{g1} + k_{g2} f_{g2} + k_{\text{int}} f_{\text{int}} \\ k_1, k_2 = 0, \pm 1, \pm 2, \cdots \\ kg_1 = 0, 1, 2, \cdots \\ kg_2 = 0, 1, 2, \cdots \\ k_{\text{int}} = \pm 1 \\ L = |k_1| + |k_2| \\ \min(L) = 1 \end{cases}.$$

In addition to these constraints for a specific receiver, there are special cases. In Fig. 3, assume that the angle between any line and the abscissa is α, and the angle between any line and the diagonal is β. The following conclusions [28] can be drawn:

(i) Shown as Fig. 3(a)−Fig. 3(c), the horizontal lines (k_1=0) and the vertical lines (k_2=0) correspond to spurious response paths of the main receiving channel. Other lines correspond to intermodulation interference paths.

(ii) In Fig. 3, for lines satisfying $-45^\circ < \beta < 45^\circ$ and $0^\circ < \alpha < 90^\circ$, the signs of the harmonic orders of the two test signals, k_1 and k_2, are opposite.

(iii) For lines that cross the diagonal from the bottom to the top ($0^\circ < \beta < 45^\circ$, $45^\circ < \alpha < 90^\circ$), shown as Fig. 3(d), there is $k_1 > 0, k_2 < 0$; otherwise, $k_1 < 0, k_2 > 0$.

(iv) In Fig. 3(d), for the lines with β=0°(α=45°), which represent intermodulation paths, we have $|k_1|=|k_2|$ and $k_1 = -k_2$. For the lines above the diagonal, $k_1 > 0$; otherwise, $k_1 < 0$.

(v) For lines satisfying $45^\circ < \beta < 135^\circ$ and $90^\circ < \alpha < 180^\circ$, the signs of k_1 and k_2 are both positive as shown in Fig. 3(d).

2.2.2 Prediction of nonlinear interference response in frequency and power domains

The existing dual-frequency test method only pays attention to the nonlinear response related to frequency. However, on the large platform or in complex system, the majority of the devices are surrounded by the strong electromagnetic field, leading to the unexpected signals coupled to the receiver input port of strong power [29], the nonlinear effects of which should not be ignored, especially when the receiver selectivity is not ideal. Therefore, modeling the receiver's nonlinear sensitivity in the frequency domain and power domain respectively is studied in this subsection. By extracting the values on the intermodulation paths from the IF response diagram and mathematically analyzing them, the frequency constraint equations [30] and the frequency-power fitting curve of the interference response will be obtained.

The extraction process is shown in Fig. 4. Only two

points on the line are needed to extract all measured values on an intermodulation path. After selecting one point, the extraction software will get the coordinate of that point. Similarly, by choosing another point on the same line, the extraction software will get the data of all points on the line determined by these two points. The extracted data are composed of the frequency on the horizontal axis, frequency on the vertical axis and measured power distinguished by color.

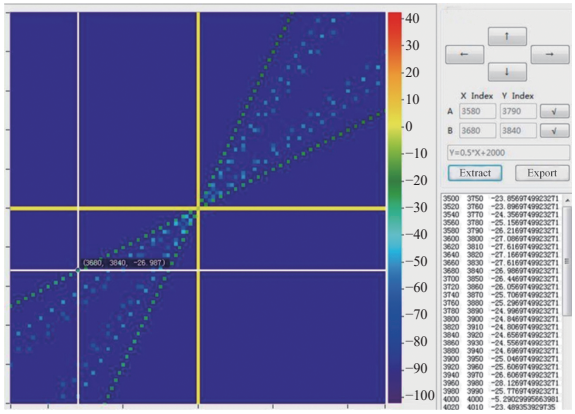

Fig. 4 Schematic of data extraction method on intermodulation inference response

The frequency constraint equation of the interference response can be determined by image interpretation illustrated in Subsection 2.2.1. Here, the derivation of the prediction model of the receiver output power is emphatically introduced. The receiver sensitivity model, consists of a nonlinear part and a linear part. The linear region is determined by the linear amplifier and the IF filter, which can be expressed as

$$P_{\text{out}} = A_{\text{int}}(f) \cdot x(f) \tag{1}$$

where $x(f)$ is the input signal with frequency f and $A_{\text{int}}(f)$ is the linear part of the gain related to the frequency.

For the nonlinear part, considering nonlinear components of k_1, k_2, k_{g1}, and k_{g2} orders, there is

$$k_1 f_1 + k_2 f_2 = k_{g1} f_{g1} + k_{g2} f_{g2} + k_{\text{int}} f_{\text{int}}. \tag{2}$$

It can be seen that f_1 and f_2 are independent, the nonlinear output of k_1,k_2,k_{g1}, and k_{g2} can be written as the function of f_1:

$$y_{k_1,k_2,k_{g1},k_{g2}} = \sum_{n=1}^{\infty} A_1(f_1) f_1^n, \tag{3}$$

$$f_2 = (k_{g1} f_{g1} + k_{g2} f_{g2} + k_{\text{int}} f_{\text{int}} - k_1 f_1) \cdot k_2^{-1}, \tag{4}$$

where A_1 is coefficient of each nonlinear order, and k_1, k_2, k_{g1}, and k_{g2} are known for a specific order. The sensitivity model of the receiver can thus be written as

$$P_{\text{out}}^{k_1,k_2,k_{g1},k_{g2}} = A_{\text{int}}(k_{\text{int}} f_{\text{int}}) \cdot \sum_{n=1}^{\infty} A_1(f_1) f_1^n. \tag{5}$$

Combine the coefficients in (5) and there is

$$P_{\text{out}}^{k_1,k_2,k_{g1},k_{g2}} = \sum_{n=1}^{\infty} A_{\text{int}}(k_{\text{int}} f_{\text{int}}) \cdot A_1(f_1) f_1^n = \sum_{n=1}^{\infty} A_n^{k_1,k_2,k_{g1},k_{g2}}(f_1) f_1^n. \tag{6}$$

Therefore, only $A_n^{k_1,k_2,k_{g1},k_{g2}}(f_1)$ is required to be measured to establish the receiver sensitivity model in power domain.

3. Experiment

To verify the proposed method, an experiment on a radar receiver is performed to detect and predict its nonlinear sensitivity. The structure of the receiving channel is shown in Fig. 5.

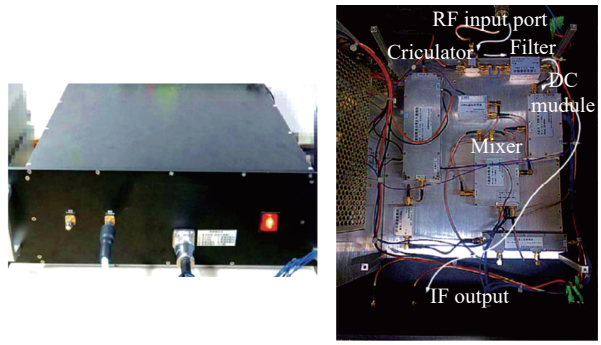

(a) Receiver photograph (b) Diagram of receiving channel

Fig. 5 Layout diagram of the radar receiver

As indicated by the arrow, the RF signal enters the receiving channel through the circulator and then passes through the filter into the down-conversion (DC) module. Finally, the signal is transferred to IF and output. The experiment is conducted under conditions listed in Table 1.

Table 1 Key parameters of the radar receiver system

Parameter	Value
Input frequency/MHz	2 300−2 400
Input power/dBm	[−90, −60]
IF output frequency/MHz	45±15
The first IF/MHz	2 180
The second IF/MHz	175
Output power/dBm	[−30, −0]
Spur rejection for IF output/dB	>60
Local suppression/dB	>60

The experiment setup of the receiver nonlinearity measurement is shown in Fig. 6. Agilent E8267D signal generators generate the two original excitation signals. The signals are then injected in combination into the receiver's RF receiving channel, mixed by broadband circuit combiner. Agilent E4447A spectrometer is used here to detect the IF output power of the receiver. The Matlab program controls the whole process, including frequency scanning, IF output measurement, and data storage.

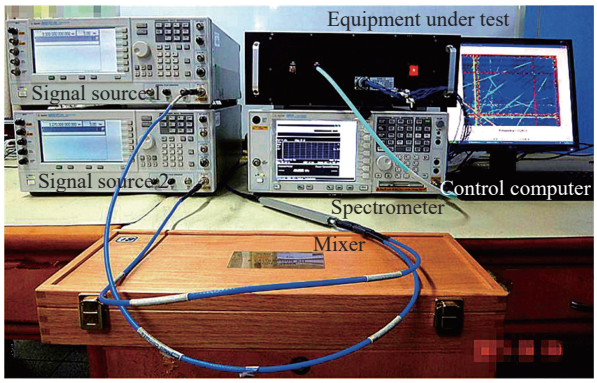

Fig. 6 Layout of the experiment of measuring the receiver nonlinearity

Considering the in-band and out-band nonlinearity of the receiver, we set the measurement frequency band as 1−3.5 GHz to obtain the model in the broadband range. To guarantee data acquisition speed at the same time, the frequency band from 1 GHz to 3.5 GHz is divided into three parts, 1−2.3 GHz, 2.3−2.5 GHz, and 2.5−3.5 GHz. Among them, 2.3−2.5 GHz covers the receiver working frequency, thus is called in-band frequency, and the other two are called out-band frequencies. Because sensitivities of in-band and out-band frequencies are different, at least measurement data in 1−2.3 GHz and 2.3−2.5 GHz should be analyzed to draw the conclusion completely.

3.1 Analysis of frequency band 1−2.3 GHz

The sweep frequency range of two signal sources is set as 1−2.3 GHz, and the output power level of the signal source is set as 5 dBm. Test results of IF response are shown in Fig. 7. Fig. 7(a) corresponds to a signal scanning step of 26 MHz, containing a total of 51×51 frequency combinations.

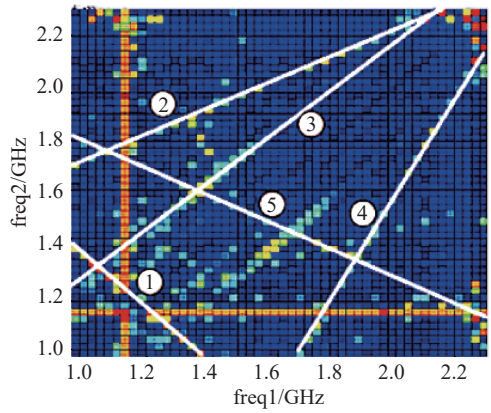

(a) Tested with a frequency scanning step of 26 MHz (two-dimensional)

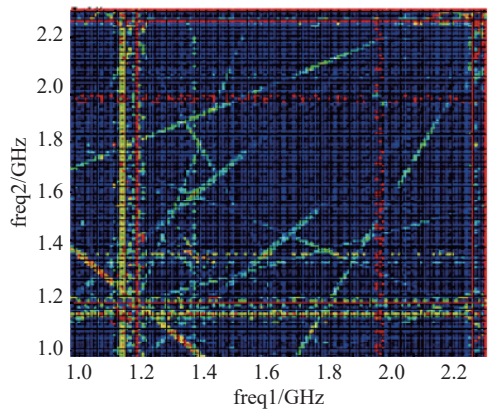

(b) Tested with a frequency scanning step of 10 MHz (two-dimensional)

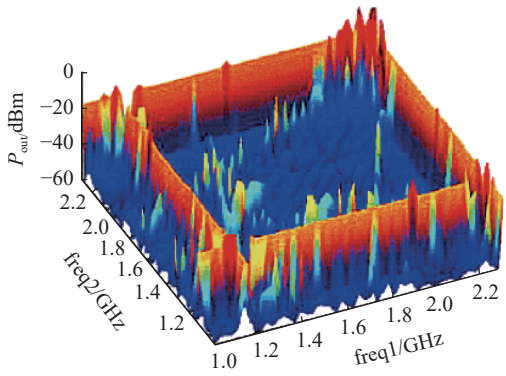

(c) Tested with a frequency scanning step of 26 MHz (three-dimensional)

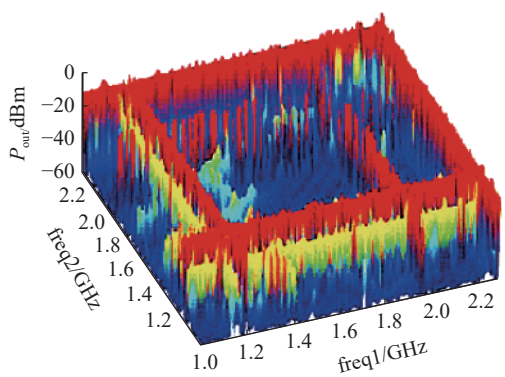

(d) Tested with a frequency scanning step of 10 MHz (three-dimensional)

Fig. 7 Tested IF out-band output response in two-dimension and three-dimension

We select five main frequency response lines. The frequency constraint equation and intermodulation order corresponding to each line is obtained by data extraction and post-processing, as detailed in Table 2.

Table 2 Characteristics of interference lines and corresponding frequency constraint equations of the tested secondary-superheterodyne receiver with input signal frequency 1−2.3 GHz

Line	k_1	k_2	L	k_{g1}	k_{g2}	f_{int}/MHz	Constraint equation
①	1	1	2	1	3	49	freq2=−1×freq1+2 416
②	2	−1	3	0	3	59	freq2=0.5×freq1+1 215
③	−1	1	2	0	1	33	freq2=1×freq1+208
④	1	1	2	3	1	49	freq2=2×freq1−2 430
⑤	−2	3	5	0	3	59	freq2=−0. 5×freq1+2 332

From Table 2, once the input frequency is determined, the interference caused by all combinations of frequencies falling into the IF operating band can be characterized by image interpretation. We can see that the interference effect caused by the combined frequencies can be represented by the frequency constraint equation. Based on the frequency constraint equation, the interference caused by each harmonic frequency and each order can be determined at a certain input frequency, thus facilitating a comprehensive understanding of the receiver's electromagnetic susceptibility.

As shown in Fig. 7(b) and Fig. 7(d), output response is detected in the same frequency band as in Fig. 7(a) and Fig. 7(c), but with a smaller signal source scanning step as 10 MHz, composed of a total of 131×131 frequency combinations. Comparing the main lines of frequency response, we can see that the response paths of larger frequency step and smaller step are consistent. Therefore, the data extracted with a large scanning step can be used for sensitivity modeling and prediction, which will shorten the time for sampling and modeling significantly.

Choosing line ③ and line ⑤ in Fig. 7(a) with different colors meaning that with different output power levels as the examples, the interference prediction models in power domain are established by polynomial curve fitting, shown in Fig. 8 and Fig. 9 respectively. That is to say, taking the signal frequency as the independent variable x of the polynomial, we can obtain the IF output power y of the signal at the corresponding frequency.

According to the sensitivity threshold of the receiver, the value of output power on the prediction curve can be used as the criterion of whether the receiver will be interfered [31]. In order to verify the credibility of the model, the fitted prediction curve and test data with a smaller scanning step (10 MHz) are both plotted in the same figure, showing good coincidence between them besides inconsistency in some small frequency parts.

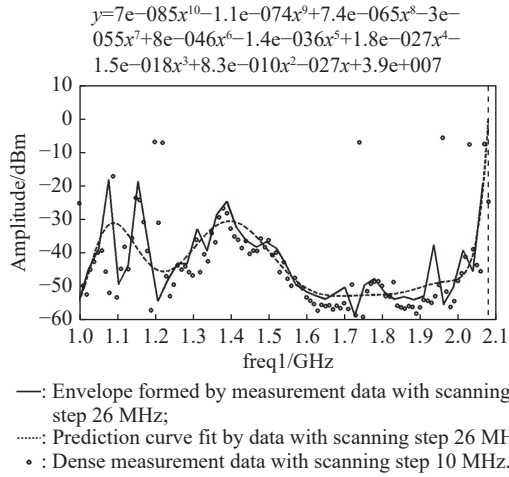

Fig. 8 IF output response prediction curve corresponding to line ③ in Fig. 7

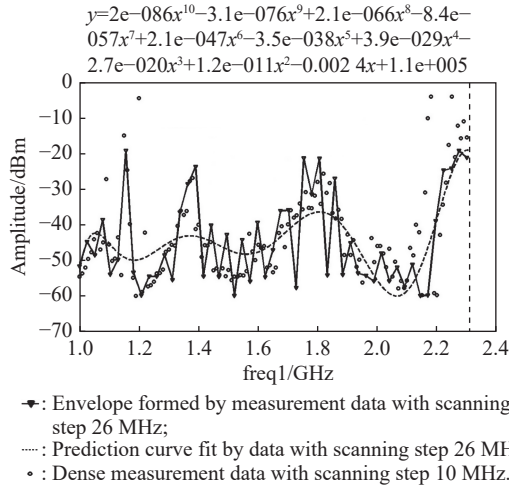

Fig. 9 IF output response prediction curve corresponding to line ⑤ in Fig. 7

In Fig. 8, differences between prediction models and measurement data appear around 1.2 GHz. This is because several response lines intersect at these frequencies, and the measurement data reflects all of the nonli-

near output components while the prediction model is established only for line ③. At the same time, two lines are orthogonal at 1.2 GHz, resulting from the RF response of the signal harmonic which is not ideally suppressed due to limited equipment conditions. Similar phenomenon exists in Fig. 9.

Despite this, models on the two lines with different harmonic and output power show good consistency overall. Therefore, the interference in the continuous frequency to the receiver can be well predicted by carrying out tests and modeling at discrete frequency points with the proposed approach.

3.2 Analysis of frequency band 2.3−2.5 GHz

Similar to measurement on out-band frequency, we set the sweep frequency band of two signal sources as 2.31−2.49 GHz, and the output power level of the signal soure as −20 dBm. Test results of IF response of in-band frequency are shown in Fig. 10. Data used for modeling is obtained with a signal scanning step of 5 MHz, containing a total of 37×37 frequency combinations, and data for validation is obtained with a scanning step of 3 MHz, containing a total of 61×61 frequency combinations.

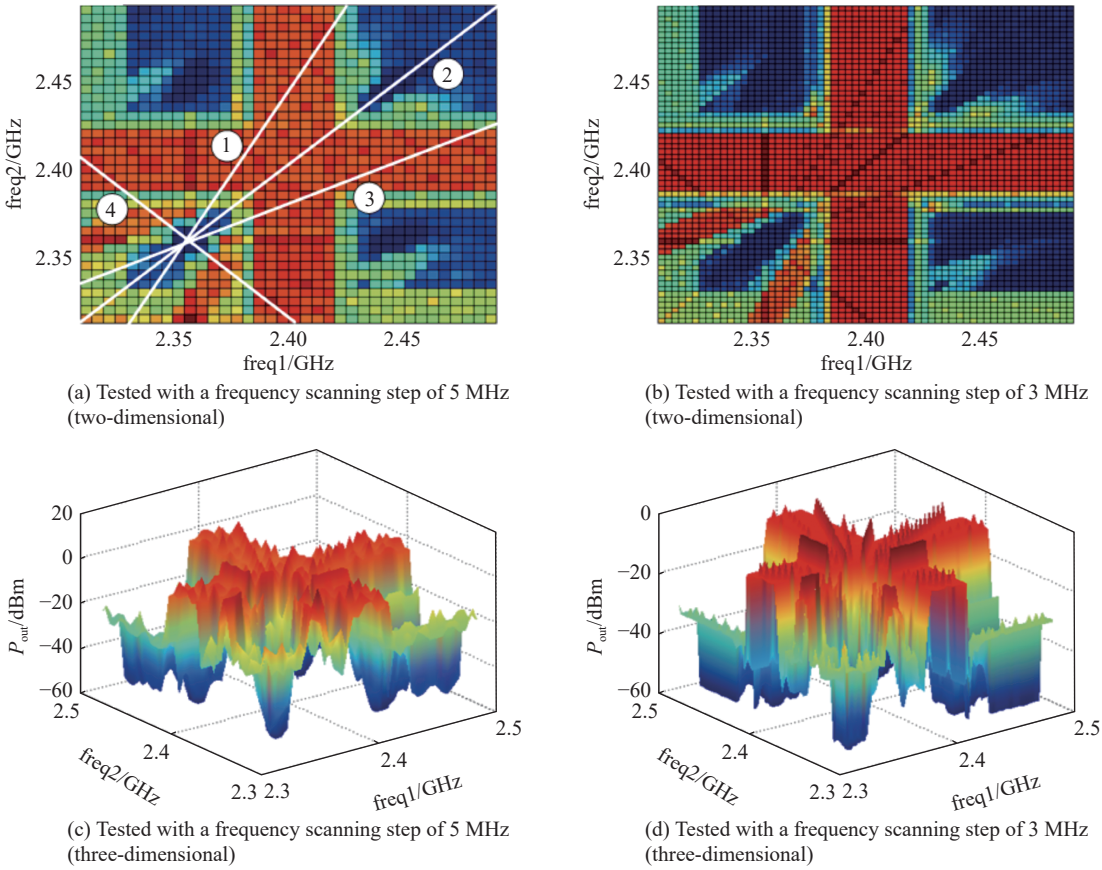

(a) Tested with a frequency scanning step of 5 MHz (two-dimensional)

(b) Tested with a frequency scanning step of 3 MHz (two-dimensional)

(c) Tested with a frequency scanning step of 5 MHz (three-dimensional)

(d) Tested with a frequency scanning step of 3 MHz (three-dimensional)

Fig. 10 Tested IF in-band output response in two-dimension and three-dimension

The cross region in Fig. 10 is where the linear response of the receiver is the strongest. In addition some nonlinear response lines in measurement data are observed.

Similar to Subsection 3.1, measurement data recorded with larger frequency step 5 MHz is analyzed to establish the prediction model. The four lines marked in Fig. 10(a) is processed to determine the harmonic orders and frequency constraints. The results are listed in Table 3.

Table 3 Characteristics of interference lines and corresponding frequency constraint equations of the tested secondary-superheterodyne receiver with input signal frequency 2.3−2.5 GHz.

Line	k_1	k_2	L	k_{g1}	k_{g2}	f_{int}/MHz	Constraint equation
①	−3	3	6	0	1	55	freq2=2×freq1−2 350
②	−2	3	5	1	1	45	freq2=freq1
③	0	1	1	1	3	47	freq2=0.5×freq1+1 285
④	−3	3	6	0	1	35	freq2=−freq1+4 720

Corresponding to line ② and line ③ in Fig. 10(a), the interference prediction models in power domain are established by polynomialcurve fitting, shown in Fig. 11 and Fig. 12 respectively.

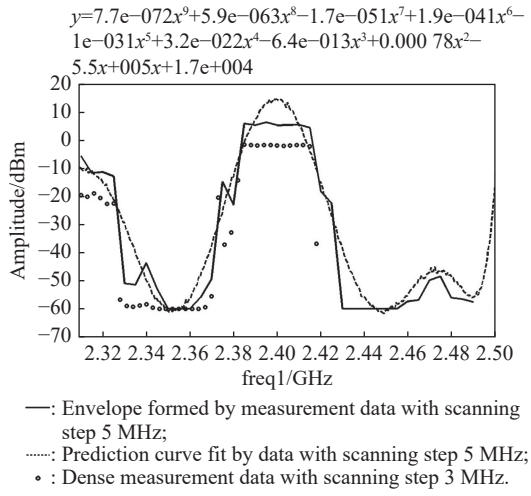

Fig. 11 IF output response prediction curve corresponding to line ② in Fig. 10

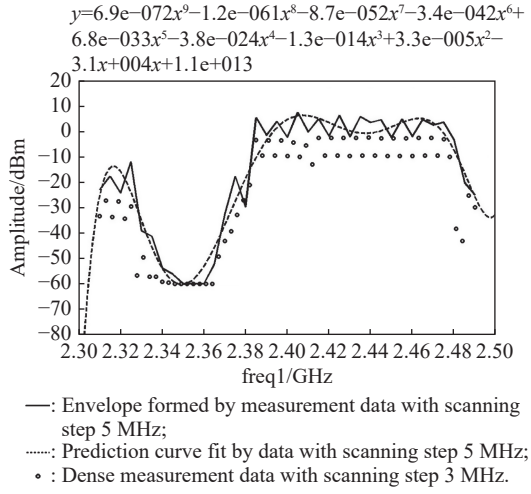

Fig. 12 IF output response prediction curve corresponding to line ③ in Fig. 10

In the work band, IF response of the working signals takes a major part, resulting in a relatively gentle in-band output. As shown in Fig. 11 and Fig. 12, the fitted prediction curves meet well with the measurement data.

Therefore, based on the frequency constraint equation of the transmission channel and the curve fitting equation in power domain, we can predict which harmonic order and how strong the power is will interfere the receiver. This will provide strong support for frequency allocation and spectrum management of the receiver.

4. Conclusions

Theoretical analysis and experiments show that, compared with existing methods in literature, the proposed method has advantages in the following three aspects.

(i) Test excitation signal with various frequency combinations generated by dual channel and the scanning frequency method with large frequency step make it be able to quickly obtain comprehensive receiver immunity characteristic parameters of sample data and rapidly detect all kinds of new frequency components formed at the port of the receiver (or module), which assists us to trace the interference process.

(ii) All parameters of useful signals and parameters related to nonlinear effects can be detected, identified, and measured quickly.

(iii) The frequency constraint of the receiver in the continuous frequency band are modeled with the measured data at discrete, finite frequency points obtained by large-step scanning. Its accuracy has been verified by comparing with the stepwise accurate frequency measurement. Furthermore, the prediction models can effectively determine whether the input signal will interfere with the receiver under a certain interference path from the power domain, thus realizing the prediction of the interference characteristics in the continuous frequency range by the discrete measurement data of finite frequency points.

In conclusion, the method proposed in this paper works effectively and efficiently in the acquisition of receiver interference response data, interpretation of interference types and related parameters, and prediction of interference sensitivity under complex electromagnetic environment, making it competitive to replace the conventional method based on human experience. Thus, the proposed method can greatly improve the accuracy and efficiency of analyzing and solving electromagnetic interference problems, which will have guiding significance for the measurement, analysis, and prediction of EMC of large platforms.

References

[1] MORDACHEV V, SINKEVICH E, TSYANENKA D, et al. EMC diagnostics of complex ship radioelectronic systems by the use of analytical and numerical worst-case models for spurious EM couplings. Proc. of the International Symposium on Electromagnetic Compatibility, 2019: 214−219.

[2] ZHANG Q L, WANG Y M, CHENG E W, et al. Investigation on in-band interference effect and out-of-band interference mechanism of B1I navigation receiver. Radioengineering, 2021, 30(3): 584–592.

[3] HU Q, CAO J Y, GAO G M Y, et al. Study of an evaluation model for AIS receiver sensitivity measurements. IEEE

Trans. on Instrumentation & Measurement, 2020, 69(4): 1118–1126.

[4] CHEN Z. Nonlinearity study of receiver in complex electromagnetic environment. Chengdu: University of Electronic Science and Technology of China, 2011. (in Chinese)

[5] YIN W J, WEN T. Study on EMI analysis and inhibitory techniques for switching converter devices. Progress in Electromagnetics Research Letters, 2019, 85: 59–64.

[6] PECCARELLI N, PECK Z, GARRY J L. Analysis and mitigation of receiver induced nonlinearities on Pulse-Doppler radars. Proc. of the IEEE International Radar Conference, 2020: 333−338.

[7] SINKEVICH E. Worst case model for fast analysis of intermodulation interference in radio receiver. Proc. of the International Symposium on Electromagnetic Compatibility, 2020. DOI: 10.1109/EMCEUROPE48519.2020.9245732.

[8] MARDIGUIAN M. Combined effects of several simultaneous EMI couplings. Proc. of the IEEE International Symposium on Electromagnetic Compatibility, 2000: 21–25.

[9] DUFFY A, ORLANDI A, ARMSTRONG K. Preliminary study of a reverberation chamber method for multiple-source testing using intermodulation. IET Science, Measurement & Technology. 2010, 4(1): 21–27.

[10] ZANG H. Research on in-band EMC test method of RF receiver. Proc. of the IEEE 6th International Symposium on Electromagnetic Compatibility, 2019. DOI: 10.1109/ISEMC-48616.2019.8986144.

[11] LAND OP'T, SJOERD T, RAMDANI M, et al. Simple, Taylor-based worst-case model for field-to-line coupling. Progress in Electromagnetics Research, 2013, 140: 297–311.

[12] DUFF W G. Electromagnetic compatibility in telecommunications. Gainesville: Interference Control Technokogies, Inc., 1988.

[13] HUNTER J, XIA S, HARMON A, et al. Modeling and statistical characterization of electromagnetic coupling to electronic devices. Proc. of the United States National Committee of URSI National Radio Science Meeting, 2021: 14−15.

[14] CAI S X, LI Y Y, ZHU H, et al. A novel electromagnetic compatibility evaluation method for receivers working under pulsed signal interference environment. Applied Sciences, 2021, 11: 9454.

[15] SINKEVICH E, MORDACHEV V, GALENKA A, et al. Fast EMC diagnostics of complex on-board radio systems with use of experimentally refined worst-case and conditionally worst-case models of “transmitter-to-receiver” interactions. Proc. of the IEEE International Joint EMC/SI/PI and EMC Europe Symposium, 2021: 208−213.

[16] SVISTUNOU A, MORDACHEV V, SINKEVICH E, et al. Analysis of EMC between medical short-range devices and equipment of wireless systems. Proc. of the IEEE International Joint EMC/SI/PI and EMC Europe Symposium, 2021: 214−219.

[17] HEITER G L. Characterization of nonlinearities in microwave devices and systems. IEEE Trans. on Microwave Theory and Techniques, 1973, 21(12): 797–805.

[18] XU J, WU J H. Automatic measurement of mixer intermodulation characteristics. Chinese Journal of Electron Devices, 2008, 31(2): 698–701. (in Chinese)

[19] ZHANG L H, YIN Y D. Fast automatic intermodulation measurement system for radio-frequency circuits. Instrument Technique and Sensor, 2014(4): 56–59. (in Chinese)

[20] WEI J Y. The non-linear distortion in radar receiver. Modern Radar, 1998, 20(1): 94–104. (in Chinese)

[21] HANDEL P, ZETTERBERG P. Receiver I/Q imbalance: tone test, sensitivity analysis, and the universal software radio peripheral. IEEE Trans. on Instrumentation and Measurement, 2010, 59(3): 704–714.

[22] SINKEVICH E. Extraction of frequency response of receiver input filter from characteristic of receiver susceptibility to third-order intermodulation. Proc. of the International Symposium on Electromagnetic Compatibility, 2017. DOI: 10.1109/EMCEUROPE.2017.8094692.

[23] TAN H, HUANG M L. Numerical simulation of the nonlinear response of receiver mixer. Proc. of the International Applied Computational Electromagnetics Society Symposium, 2017: 1−3.

[24] WU W, TAN H. Behavioral modeling and simulation of electromagnetic interference response for radio frequency receiver. Proc. of the IEEE 6th International Symposium on Microwave, Antenna, Propagation, and EMC Technologies, 2015: 405−408.

[25] XING K, XUE M L, WANG Y W, et al. Application of wireless receiver ’s EMC fast testing technique in complicated electromagnetic environment. Journal of Astronautic Metrology and Measurement, 2015, 35(5): 21–26. (in Chinese)

[26] MORDACHEV V I. Automated double frequency test system. Proc. of the International Conference on Electromagnetic Interference and Compatibility '99, 1997: 99−104.

[27] MORDACHEV V, SINKEVICH E, PETRACHKOV D. Representation and analysis of radio receivers’ susceptibility and nonlinearity by the use of 3D double-frequency characteristics. Proc. of the International Symposium on Electromagnetic Compatibility, 2014: 689−692.

[28] MORDACHEV V I. Automated double-frequency testing technique for mapping receive interference responses. IEEE Trans. on Electromagnetic Compatibility, 2000, 42(2): 213–225.

[29] MA Y L, YAMAO Y. Blind nonlinear compensation technique for RF receiver front-end. Proc. of the European Microwave Integrated Circuit Conference, 2013: 556−559.

[30] MA C. Research on double-multiple frequency testing technology and application. Changsha: National University of Defense Technology, 2013. (in Chinese)

[31] MAOULOUD A, KLINGLER MBESNIER P. A test bench for measuring the sensitivity threshold of FM receivers in the presence of interference through direct injection of the radio signal. Proc. of the International Symposium on Electromagnetic Compatibility, 2020. DOI: 10.1109/EMCEUROPE48519.2020.9245696.

Biographies

CHEN Yan was born in 1991. She received her B.S. degree in electronic information science and technology from the University of Electronic Science and Technology of China in 2015 and M.S. degree in electronic science and technology from the National University of Defense Technology (NUDT) in 2017. After that, she has been working as an aerospace engineer in the State Key Laboratory of Astronautic Dynamics, Xi'an, China. She is pursuing her Ph.D. degree in the State Key Laboratory of Complex Electromagnetic Environment Effects on Electronics and Information System, NUDT, Changsha, China. Her research interests include complex detection equipment management, assessment, and resource scheduling.
E-mail: chenyancy@nudt.edu.cn

LU Zhonghao was born in 1983. He received his M.S. and Ph.D. degrees in electronic science and technology from National University of Defense Technology (NUDT), Changsha, China, in 2008 and 2013, respectively. He is an associate professor with NUDT. His current research interests include microwave devices design, antenna design, and electromagnetic compatibility testing.
E-mail: luzhonghao@nudt.edu.cn

LIU Yunxia was born in 1978. She received her B.S. and M.S. degrees in control theory and control engineering from Harbin Engineering University in 2003 and 2006, respectively. She worked as a design engineer in Jinan Worldwide Auto-Accessory Limited from 2006 to 2011. After that, she worked as an electrical design senior engineer in China National Petroleum Corporation Jichai Power Company Limited from 2011 to 2019. She is currently an aerospace engineer in State Key Laboratory of Astronautic Dynamics, Xi'an, China. Her research interests include radar performance evaluation and resource scheduling.
E-mail: lyxhello1209@126.com